Atmos. Chem. Phys., 25, 10731–10745, 2025
https://doi.org/10.5194/acp-25-10731-2025

Atmospheric Chemistry and Physics
Open Access
EGU

Roles of pH, ionic strength, and sulfate in the aqueous nitrate-mediated photooxidation of green leaf volatiles

Yuting Lyu[1,2], Taekyu Joo[3], Ruihan Ma[1], Mark Kristan Espejo Cabello[1,2], Tianye Zhou[1], Shun Yeung[1], Cheuk Ki Wong[1], Yifang Gu[1], Yiming Qin[1], and Theodora Nah[1,2]

[1]School of Energy and Environment, City University of Hong Kong, Hong Kong SAR, China
[2]State Key of Marine Environmental Health, City University of Hong Kong, Hong Kong SAR, China
[3]Department of Earth and Environmental Sciences, Korea University, Seoul, South Korea

Correspondence: Theodora Nah (theodora.nah@cityu.edu.hk)

Received: 7 February 2025 – Discussion started: 4 March 2025
Revised: 26 June 2025 – Accepted: 1 July 2025 – Published: 18 September 2025

Abstract. Biotic and abiotic stresses can lead to terrestrial green plants releasing green leaf volatiles (GLVs), which can partition into atmospheric aqueous phases where they can undergo oxidation to form aqueous secondary organic aerosol (aqSOA). Anthropogenic emission changes have resulted in nitrate becoming an increasingly important component of atmospheric aqueous phases, which has significant implications for aqSOA formation since nitrate photolysis produces oxidants. Nevertheless, sulfate remains the main inorganic aqueous component in most regions, and thus it controls the pH and ionic strength of atmospheric aqueous phases. We report results from laboratory investigations of the effects of pH, ionic strength, and sulfate on the reaction kinetics and aqSOA formation of the aqueous nitrate-mediated photooxidation of four GLVs: *cis*-3-hexen-1-ol, *trans*-2-hexen-1-ol, *trans*-2-penten-1-ol, and 2-methyl-3-buten-2-ol. Our results showed that the aqueous reaction medium conditions, i.e., dilute cloud/fog vs. concentrated aqueous aerosol conditions, governed the effects that pH, ionic strength, and sulfate have on the GLV degradation rates and aqSOA mass yields. Most notably, reactions initiated by sulfate photolysis will have significant effects on the GLV degradation rates and aqSOA mass yields in aqueous aerosols but not in cloud/fog droplets. In addition to providing new insights into aqSOA formation from the aqueous reactions of GLVs in regions with substantial concentrations of nitrate in cloud, fog, and aqueous aerosols, this study highlights how nitrate and sulfate photochemistries can couple together to influence the reactions of water-soluble organic compounds and their aqSOA formation in aqueous aerosols, which have implications for our evaluations of aqueous organic aerosol lifetimes and composition.

1 Introduction

Biogenic volatile organic compounds (BVOCs) contribute more than 80 % of the global volatile organic compound (VOC) emissions (Guenther et al., 2012; Sindelarova et al., 2014). Isoprene and monoterpenes comprise more than half of the total annual BVOC emissions (Sindelarova et al., 2014). Since green leaf volatiles (GLVs) comprise a comparatively small fraction of total BVOCs, their chemical processes have received far less attention compared to isoprene and monoterpene. GLVs are C_5 to C_6 unsaturated organic compounds with aldehyde, alcohol, or ester functional groups (Sarang et al., 2021a). GLVs are emitted during the decomposition of C_{18} polyunsaturated fatty acids in leaves when vegetation is exposed to herbivores, pathogens, or harsh weather conditions (Ameye et al., 2018; Matsui and Engelberth, 2022; Silva et al., 2021). They are also emitted by cyanobacteria and algae during bloom events (García-Plazaola et al., 2017). GLVs have the potential to contribute substantially to the local secondary organic aerosol (SOA) budget due to their increased emissions when vegetation is subjected to biotic and abiotic stresses. A previous study reported that GLV emissions from Amazon tropical forests increased significantly in the af-

ternoon due to the plants' response to rising temperatures, whereas isoprene and monoterpene emissions decreased (Jardine et al., 2015). Global GLV emissions will potentially increase in the future due to climate change and the increasing use of new fumigation-based agricultural, horticultural, and forestry practices (Cofer et al., 2018; Matsui and Engelberth, 2022; Su et al., 2020). Thus, GLVs may play increasingly important roles in atmospheric chemistry, which necessitates increasing our knowledge of their multiphase reactions and SOA formation.

GLVs can be oxidized by ozone and hydroxyl radicals (•OH) in the gas phase to produce low-volatility products, with reported SOA mass yields ranging from 0.7 % to 20 % (Hamilton et al., 2009; Harvey et al., 2014; Jaoui et al., 2012; Mentel et al., 2013). Due to their moderately high water solubilities, GLVs can dissolve into atmospheric aqueous phases (e.g., aqueous aerosols, cloud and fog droplets), where they can be oxidized by aqueous oxidants such as •OH, sulfate anion radicals (SO_4•$^-$), nitrate radicals (NO_3•), triplet organic excited states ($^3C^*$), and singlet oxygen ($^1O_2^*$) (Richards-Henderson et al., 2014, 2015; Sarang et al., 2021a, b, 2023). Higher quantities of low-volatility products are formed from aqueous reactions compared to gas-phase reactions, with previous studies reporting aqueous SOA (aqSOA) mass yields as high as 88 %, though this will depend on the GLV and the aqueous oxidant (Richards-Henderson et al., 2014, 2015). However, these previous studies were mostly conducted under dilute aqueous conditions mimicking aqueous cloud/fog droplets. Differences in the physicochemical properties of the aqueous reaction medium will impact reaction rates in cloud/fog droplets vs. aqueous aerosols (Herrmann et al., 2015), but little is currently known about the aqueous oxidation of GLVs under more concentrated aqueous-aerosol-like conditions.

The liquid water concentrations (LWCs) of cloud and fog droplets typically fall in the range of 0.05 to 0.5 g m^{-3} (Achtert et al., 2020; Kim et al., 2022; Korolev et al., 2007), whereas the LWCs of aqueous aerosols fall in the range of 10^{-7} to 10^{-3} g m^{-3} (Herrmann et al., 2015). Thus, the concentrations of dissolved organic and inorganic compounds are higher in aqueous aerosols, with their dry masses close to the liquid water mass (Nguyen et al., 2016). The concentrations of inorganic ions, particularly nitrate and sulfate, primarily govern the acidities and ionic strengths of atmospheric aqueous phases. Cloud and fog droplets (pH 2 to 7) are generally less acidic than aqueous aerosols (pH 0 to 5) due to the more frequent ammonia dissolution and higher buffering capacities of cloud and fog droplets (Pye et al., 2020; Tilgner et al., 2021). The ionic strengths of atmospheric aqueous phases span a large range (10^{-5} to 10^{0} M), with the ionic strengths of aqueous aerosols being several orders of magnitude higher than those of cloud and fog droplets (Herrmann et al., 2015; Tilgner et al., 2021). Under the high-ionic-strength conditions in aqueous aerosols, substantial ion association occurs, which will affect the activity coefficients of organic compounds, resulting in reactions occurring under non-ideal conditions (Herrmann, 2003). Previous studies have reported that ionic strength significantly affects the aqueous reactions of some organic compounds and subsequent product formation (Herrmann, 2003; Mekic et al., 2018a, b; Mekic and Gligorovski, 2021; Zhou et al., 2019). In addition to contributing to the acidity and ionic strength of atmospheric aqueous phases, inorganic nitrate and sulfate can undergo photolysis to produce various reactive species that react with organic compounds. The tropospheric irradiation of nitrate in atmospheric aqueous phases is known to produce aqueous reactive species such as •OH, nitric oxide radicals (NO•), and nitrogen dioxide radicals (NO_2•) that can react with organic compounds (Mack and Bolton, 1999; Gen et al., 2022). Even though a recent study reported that sulfur-containing radicals (e.g., SO_4•$^-$) are formed during the tropospheric irradiation of aqueous sulfate aerosols (Cope et al., 2022), the mechanisms behind their formation are still not well understood. While nitrate is increasingly important in regions with large reductions in sulfur dioxide emissions and/or with high ammonia emissions (Heald et al., 2012; Schaap et al., 2004; West et al., 1999), sulfate remains the dominant inorganic constituent of atmospheric aqueous phases in most regions (Bianco et al., 2020). At present, little is known about how inorganic nitrate and sulfate salts influence the aqueous oxidation of GLVs.

In this study, we investigated the nitrate-mediated photooxidation of four GLVs, *cis*-3-hexen-1-ol, *trans*-2-hexen-1-ol, *trans*-2-penten-1-ol, and 2-methyl-3-buten-2-ol (Fig. 1), under cloud-/fog-like and aqueous-aerosol-like conditions. These four GLVs, which are amongst some of the more abundant GLVs, have Henry's law constants between 60 and 120 M atm^{-1} (Sander, 2023; Sarang et al., 2021a). Thus, they can partition efficiently into cloud/fog droplets and moderately into aqueous aerosols (Fig. S1 in the Supplement). We investigated the effects of pH, ionic strength, and sulfate have on the reaction kinetics and aqSOA mass yields under cloud-/fog-like and aqueous-aerosol-like conditions. Results from this study provide new insights into the aqueous photooxidation of GLVs in regions with substantial levels of nitrate in cloud and fog droplets and aqueous aerosols and, more generally, into how sulfate photochemistry impacts the aqueous nitrate-mediated photooxidation of other water-soluble organic compounds.

2 Methods

2.1 Chemicals and solutions

All the chemicals were used as received. *cis*-3-Hexen-1-ol (cHxO, 98 %), *trans*-2-hexen-1-ol (tHxO, 96 %), 2-methyl-3-buten-2-ol (MBO, 97 %), benzoic acid (BA, 99.5 %) and p-hydroxybenzoic acid (pHBA, 99 %) were purchased from J&K Scientific. *Trans*-2-penten-1-ol (tPtO, $\geq$ 95 %) was purchased from Aladdin Scientific. Ammo-

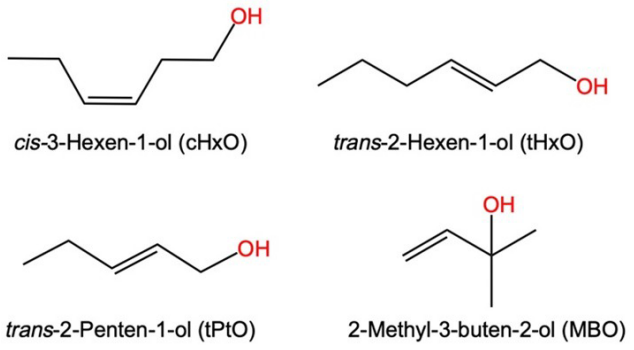

Figure 1. The four model GLVs used in this study.

nium nitrate (NH_4NO_3, $\geq 95\,\%$) and ammonium sulfate ($(NH_4)_2SO_4$, 99+ %) were purchased from Fisher Scientific. Sulfuric acid (H_2SO_4, 95 %) was purchased from VWR Chemicals BDH©. Milli-Q ultrapure water (18.2 MΩ cm) was used to prepare all solutions.

Table 1 shows the concentrations of solutions used to simulate cloud-/fog-like and aqueous-aerosol-like conditions in photochemistry experiments. The same nitrate / GLV molar concentration ratio (i.e., 2.5 : 1) was used for both cloud-/fog-like and aqueous-aerosol-like conditions. The concentrations of the GLVs and NH_4NO_3 were set to be 100 times higher for the aqueous-aerosol-like conditions than the cloud-/fog-like conditions. The nitrate concentration (i.e., 250 µM) used for cloud-/fog-like conditions is close to those measured in cloud water in Hong Kong SAR (average of 238 µM) (Li et al., 2020) and is within the global range for nitrate in continental cloud water (Bianco et al., 2020). Even though the nitrate concentration in aqueous aerosols could reach molar levels (Bzdek et al., 2020), we used 25 mM of NH_4NO_3 in experiments that simulate aerosol-like conditions to maintain the same nitrate / GLV molar concentration ratio as in experiments that simulate cloud-/fog-like conditions. The pH levels of unbuffered solutions (no addition of H_2SO_4) were close to 5, and 5 was selected as the higher bound to study the pH effects on the nitrate-mediated photooxidation of GLVs. The lower bound of pH was set to 3 through the addition of H_2SO_4. $(NH_4)_2SO_4$ was added into the solutions to control the sulfate concentrations in and ionic strengths of the solutions. Since the acid dissociation constant (pK_a) for $HSO_4^- \leftrightarrow H^+ + SO_4^{2-}$ is around 2.0 at 25 °C (Dickson et al., 1990), SO_4^{2-} is expected to be the dominant species even at the lower bound of pH 3. The pH levels (i.e., pH 3 vs. pH 5, Table 1) used in this study fall within the ranges for cloud and fog droplets and aqueous aerosols (Herrmann et al., 2015; Pye et al., 2020; Tilgner et al., 2021). The ionic strengths (I_{total}) of the solutions were calculated using the following equation:

$$I_{total} = \frac{1}{2} \times \sum_{i=1}^{i=n} c_i z_i^2, \quad (1)$$

where c_i and z_i are the concentration (M) and charge, respectively, of inorganic ion i for H^+, NH_4^+, NO_3^-, and SO_4^{2-}. The ionic strengths used in this study, i.e., 0.002 M vs. 0.02 M for cloud-/fog-like conditions and 0.5 M vs. 3.3 M for aqueous-aerosol-like conditions (Table 1), fall within the ranges for ionic strengths for clouds/fog droplets and continental aerosols (Herrmann et al., 2015). Only the addition of tPtO and tHxO had significant effects on the molar absorptivity of NH_4NO_3 (Fig. S2b), enhancing the peak molar absorptivity of NH_4NO_3 approximately 1.3- and 1.5-fold, respectively.

2.2 Photochemistry experiments

The solutions were placed into open cylindrical quartz tubes (1.2 cm inner diameter), which were placed on a rotating sample holder located in the middle of a photoreactor (Rayonet RPR-200, Southern New England UV Co.) surrounded by UVB lamps (RPR-3000Å, Southern New England UV Co.). The photon flux in the photoreactor ranged from 250 to 400 nm and peaked at 311 nm (Fig. S2a). The temperature inside the photoreactor during experiments was maintained at around 30 °C by a cooling fan located at the bottom of the photoreactor. The volume of each quartz tube was around 15 mL. The quartz tubes were filled with 10 and 1 mL of solutions during experiments simulating cloud-/fog-like and aqueous-aerosol-like conditions, respectively. Aliquots of 1 and 0.1 mL were extracted from the illuminated solutions at different reaction times for offline chemical analysis during experiments simulating cloud-/fog-like and aqueous-aerosol-like conditions, respectively. For experiments simulating aqueous-aerosol-like conditions, the extracted volume (0.1 mL) was diluted with Milli-Q ultrapure water by a factor of 10 prior to chemical analysis to ensure that the measured signals stayed within the linear detection range of the detector. The decays of the GLVs were measured using an ultrahigh-performance liquid chromatograph coupled to a photodiode array detector (UPLC-PDA, H-class, Waters). A Kinetex Polar C18 column (2.6 µm, 100 × 2.1 mm) equipped with a security guard and Polar C18 pre-column was used for the measurement of the four GLVs. An isocratic elution program set to 0.3 mL min^{-1} was used. The mobile phases of water and acetonitrile were run at a ratio of 80 : 20 for cHxO, tHxO, and MBO and at a ratio of 85 : 15 for tPtO. The detection wavelengths were set to 240 nm for MBO and 210 nm for the other three GLVs. All the experiments and measurements were performed three times. All the decays of the GLVs followed apparent first-order reaction kinetics reasonably well (Figs. S3 and S4); thus they were fitted with the following equation:

$$\ln\left(\frac{[GLV]_t}{[GLV]_0}\right) = -k_{obs}t, \quad (2)$$

where k_{obs} is the pseudo-first-order rate obtained from the exponential fit to the photodegradation of the GLV and

Table 1. Concentrations of GLVs, NH_4NO_3, H_2SO_4, $(NH_4)_2SO_4$, the pH, and I_{total} of solutions used to simulate cloud-/fog-like and aqueous-aerosol-like conditions in photochemistry experiments.

Simulated condition	[GLV] (mM)	[NH_4NO_3] (mM)	[H_2SO_4] (mM)	pH	[$(NH_4)_2SO_4$] (mM)	I_{total} (M)
Cloud-/fog-like	0.1	0.25	0.5	3	0.135	0.002
					6.135	0.02
			0	5	0.583	0.002
					6.580	0.02
Aqueous-aerosol-like	10	25	0.5	3	158	0.5
					1085	3.3
			0	5	158	0.5
					1085	3.3

$[GLV]_t$ and $[GLV]_0$ are the concentrations of individual GLV measured by UPLC-PDA at illumination times t and 0, respectively.

No loss in GLVs was observed in dark control experiments conducted in the absence and presence of nitrate and sulfate. During illumination in control experiments conducted in the absence of nitrate and sulfate ("light only" experiments), only MBO had significant loss under cloud-/fog-like conditions, whereas all four GLVs had significant losses under aqueous-aerosol-like conditions (Figs. S3 and S4). The four GLVs were not expected to undergo direct photolysis as they do not absorb light significantly at wavelengths larger than 280 nm (Richards-Henderson et al., 2014; Sarang et al., 2021a), as demonstrated in Figs. S5 and S6. Thus, the observed losses under illumination in control experiments conducted in the absence of nitrate and sulfate could be due to evaporation, with MBO having the largest losses due to its higher vapor pressure (3.08×10^{-2} atm) compared to the other three GLVs (cHxO: 1.23×10^{-3} atm; tHxO: 1.20×10^{-3} atm; tPtO: 3.46×10^{-3} atm) based on estimations using EPI Suite^{TM} (US EPA, 2024). The k_{obs} values measured for the GLV decays in nitrate-mediated photooxidation experiments were subsequently corrected by subtracting the loss rates from control experiments conducted in the absence of nitrate and sulfate ("light only" experiments).

To gain insights into how concentration, pH, and ionic strength affect •OH formation during nitrate-mediated photooxidation, a separate set of experiments (i.e., GLVs were not present in the solutions) using BA (10 µM) as the •OH probe compound were conducted to estimate the steady-state concentrations of •OH ($[•OH]_{ss}$) using the same methodology as our past studies (Lyu et al., 2023; Yang et al., 2021, 2023). p-HBA, which is formed from the reaction of •OH with BA ($k_{BA+OH} = 5.9 \times 10^9\ M^{-1}\ s^{-1}$ (Herrmann et al., 2010)) at a yield of 0.17 (Anastasio and McGregor, 2001), was measured in these experiments using an ultrahigh-performance liquid chromatography system (1290 system, Agilent) coupled to a high-resolution quadrupole time-of-flight mass spectrometer (X500R QTOF MS/MS, Sciex) (UPLC-MS) equipped with an electrospray ionization (ESI) source that was operated in negative mode (Sect. S1 in the Supplement). Solid-phase extraction (SPE) using two different types of SPE cartridges (Oasis MAX, 60 mg, 3 mL, 60 µm, Waters; Bond PPL Elut, 200 mg, 3 mL, 125 µm, Agilent) was performed to remove inorganic salts from samples before UPLC-MS analysis. The estimated $[•OH]_{ss}$ values for the cloud-/fog-like and aqueous-aerosol-like conditions are shown in Fig. S7.

2.3 Mass yields of aqSOA

Aerosol mass spectrometry was used to measure the aqSOA mass yields of the four GLVs. Aliquots of 10 and 1 mL were extracted from the illuminated solutions at one GLV lifetime (i.e., $\tau = \frac{1}{k_{obs}}$, when 37 % of the initial concentration of the GLV remained) in experiments simulating cloud-/fog-like and aqueous-aerosol-like conditions, respectively (Tables S2 and S3). The time points equivalent to one GLV lifetime were determined from the aforementioned kinetic experiments. For experiments simulating aqueous-aerosol-like conditions, the extracted volume (1 mL) was diluted with Milli-Q ultrapure water by a factor of 300 prior to aerosol mass spectrometry analysis to ensure that the measured signals stayed within the linear detection range of detector. Each sample solution was injected at 10 mL h^{-1} by a syringe pump (model 100, KD Scientific) into an aerosol generation system (model 9200, Brechtel Manufacturing Incorporated), which aerosolized the solution. The atomizer system used nitrogen gas (99.999 % purity) as the carrier gas at a flow rate of 4.5 L min^{-1}. The aerosols generated were passed through an inline dryer before entering a time-of-flight aerosol chemical speciation monitor (ACSM, Aerodyne Research Inc.). All the experiments and measurements were performed three times.

The aqSOA mass yield (Y_{SOA}) was calculated using the following equation (Jiang et al., 2023; Ma et al., 2021):

$$Y_{SOA} = \frac{\text{organic mass increased}}{\text{GLV mass decreased}} = \frac{[\text{Org}]_\tau - [\text{Org}]_0}{[\text{GLV}]_0 - [\text{GLV}]_\tau}$$
$$= \frac{[\text{Org}]_{\text{ACSM},\tau} \times \frac{\left[SO_4^{2-}\right]_\tau}{\left[SO_4^{2-}\right]_{\text{ACSM},\tau}} - [\text{Org}]_{\text{ACSM},0} \times \frac{\left[SO_4^{2-}\right]_0}{\left[SO_4^{2-}\right]_{\text{ACSM},0}}}{(1 - 0.37) \times [\text{GLV}]_0}, \quad (3)$$

where [Org], [GLV], and $[SO_4^{2-}]$ are the concentrations of organics, the GLV of interest, and sulfate, respectively. The terms with ACSM as a subscript indicate the mass concentrations (in mg L^{-1}) of aerosols measured by the ACSM, which is different from the molar concentrations (mol L^{-1}) of solutions which do not have the ACSM subscripts. The subscripts τ and 0 indicate the sample solutions obtained at one GLV lifetime (Tables S2 and S3) and before illumination, respectively. The concentrations of sulfate in the solutions before and after illumination were assumed to be the same (i.e., $[SO_4^{2-}]_\tau = [SO_4^{2-}]_0$). The concentration of sulfate in each sample solution (Table 1) was used as the internal standard to scale the concentrations of organics measured by ACSM to those of the solutions. This is because sulfate is non-refractory and is expected to be collected and quantified by the ACSM, which had a capture vaporizer with a collection efficiency of 1 (Daellenbach et al., 2016; Xu et al., 2018; Joo et al., 2021). Additionally, the sulfate and organic composition in the atomized aerosols are expected to be internally mixed together (Ma et al., 2021).

3 Results and discussion

3.1 Cloud-/fog-like conditions

3.1.1 Reaction kinetics

The concentrations of the four GLVs decreased upon irradiation in the presence of nitrate and sulfate. In contrast to MBO, no decays were observed for cHxO, tHxO, and tPtO when only sulfate was present (but not nitrate) in the solutions. In the absence of nitrate, the MBO decay rates obtained in the absence and presence of sulfate were similar. The MBO decay in the absence of nitrate could be due to MBO evaporation since it has a higher vapor pressure than the other three GLVs. Overall, these results indicated that sulfate has an insignificant effect on the kinetics of the four GLVs under cloud-/fog-like conditions.

Figure 2 shows the k_{obs} values for the four GLVs upon irradiation in the presence of nitrate at different pH levels (i.e., 3 vs. 5) and ionic strengths (i.e., 0.002 M vs. 0.02 M). Separate experiments performed in the absence of GLVs and using BA as the •OH probe compound showed that the estimated $[\text{•OH}]_{ss}$ values decreased with pH under these cloud-/fog-like conditions (Fig. S7a), consistent with results reported by Lyu et al. (2023). The k_{obs} values for the four GLVs were on the orders of 10^{-5} to $10^{-4}\ \text{s}^{-1}$ for the four GLVs. The decays in the four GLVs upon irradiation in the presence of nitrate were due to the reactions of the GLVs with reactive species produced from nitrate photolysis such as •OH, NO•, and NO_2• (Table S1 in the Supplement). Even though approximately equal quantities of •OH and NO_2• are produced during nitrate photolysis (Chen et al., 2019; Zhang et al., 2021), the typical reactivities of NO_2• are 2 to 5 orders of magnitude lower than those of •OH (Ford et al., 2002; Chen et al., 2019; Zhang et al., 2021). Other reactive species produced during nitrate photolysis (e.g., hydroperoxide radicals (HO_2•) and superoxide ions (O_2^-•)) are also expected to have lower reactivities compared to •OH (Bielski et al., 1985; Mack and Bolton, 1999). Reaction with •OH was also shown to be the main contributor to the reaction kinetics of other non-photolyzable organic compounds (e.g., formic acid, glycolic acid) during aqueous nitrate-mediated photooxidation (Lyu et al., 2023). While it is possible that sulfur-containing radicals and other reactive species were formed from the photolysis of $(NH_4)_2SO_4$ (Table S4), their effects on k_{obs} are small due to their low concentrations under diluted cloud-/fog-like conditions (Cope et al., 2022). Additionally, the k_{obs} values measured under illumination in control experiments conducted in the presence of sulfate only were not statistically different ($p > 0.05$) from the k_{obs} values measured under illumination in control experiments conducted in the absence of nitrate and sulfate ("light only" experiments). Thus, the decays of the GLVs were likely governed mostly by their reactions with •OH, though minor contributions from their reactions with reactive species other than •OH cannot be discounted.

Under the same ionic-strength conditions, the four GLVs had higher k_{obs} at pH 3 than at pH 5, though the pH-dependent trends for cHxO at $I_{total} = 0.002$ M and 0.02 M were statistically insignificant ($p > 0.05$) (Table S5). The four GLVs do not have acidic H atoms; thus they do not undergo acid dissociation to form different relative abundances of deprotonated and neutral forms with different reactivities at different pH levels. Additionally, Richards-Henderson et al. (2014) showed that the •OH rate constants for many GLVs do not depend on pH. Hence, the pH-dependent k_{obs} trends seen in Fig. 2 were due to the pH-dependent formation of •OH (Fig. S7) and other reactive species from nitrate photolysis. HNO_2, whose production from nitrate photolysis is favored over NO_2^- production at pH $\leq$ 3.5 (Marussi and Vione, 2021), has a higher quantum yield for •OH formation than NO_2^- in the near-UV region (Arakaki et al., 1999; Marussi and Vione, 2021). Thus, the formation rates and concentrations of •OH produced at pH 3 are higher than at pH 5, which would explain the higher k_{obs} at pH 3. There were no statistically significant differences in the k_{obs} values for I_{total} of 0.002 M vs. 0.02 M under the same pH conditions for the four GLVs ($p > 0.05$). This indicated that ionic strength (and sulfate) has an insignificant effect on the reaction kinetics of the four GLVs under cloud-/fog-like conditions. Overall, only pH impacted the reaction kinetics of the four GLVs significantly under cloud-/fog-like conditions.

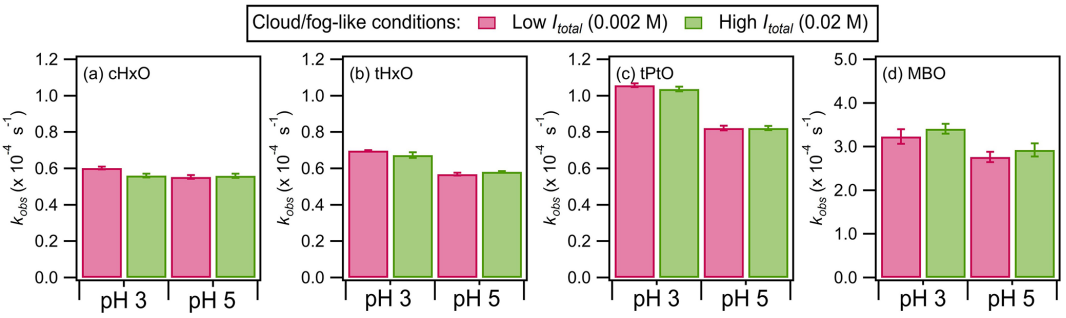

Figure 2. The k_{obs} values for the four GLVs during nitrate-mediated photooxidation under cloud-/fog-like conditions (Table 1). The error bars represent 1 standard deviation originating from triplicate experiments and measurements. Statistical analyses (Student's t test) on the differences in the k_{obs} values are presented in Tables S6 to S9.

3.1.2 Mass yields of aqSOA

Figure 3 shows the Y_{SOA} values for the four GLVs measured at one GLV lifetime during irradiation in the presence of nitrate at different pH levels (i.e., 3 vs. 5) and ionic strength (i.e., 0.002 M vs. 0.02 M). The measured Y_{SOA} values (0 % to 53 %) are in line with the range of Y_{SOA} values (10 % to 88 %) measured by Richards-Henderson et al. (2014) for five GLVs (including cHxO and MBO) at one GLV lifetime in their reactions with •OH generated from H_2O_2 photolysis under cloud-/fog-like conditions.

Given the high reactivity of •OH, reactions of the GLVs with •OH are expected to produce products that contribute substantially to aqSOA formation. However, we cannot discount the possibility that other reactive species produced from nitrate/sulfate photolysis (Tables S1 and S4) also contributed to aqSOA formation. The reaction of •OH with the GLV is expected to occur either by •OH addition to the C=C bonds to form hydroxy alkyl radicals or by H abstraction from the C–H or O–H bonds to form alkyl radicals (Figs. S8 and S9). The H-bond dissociation energies at the CH_2, CH_3, and OH groups are around 393, 419, and 436 kJ mol^{-1}, respectively (Benson, 1976). H abstraction is expected to occur preferentially at C–H sites on the carbon α to the OH group (Cooper et al., 2009; Sarang et al., 2023). The hydroxy alkyl radicals and alkyl radicals subsequently react with O_2 to form peroxy radicals (RO_2•), which then react with other RO_2• to form either higher-molecular-weight carbonyls and alcohols or alkoxy radicals (RO•). RO• can undergo fragmentation reactions to form lower-molecular-weight compounds. Even though they are not shown in our proposed reaction mechanisms in Figs. S8 and S9, bimolecular combination reactions involving RO_2• and RO• (e.g., $RO_2• + RO_2•$) that form oligomers could have also contributed to aqSOA formation.

Attempts to identify prominent low-volatility products (and their formation pathways) that contributed to aqSOA using liquid chromatography–mass spectrometry were unsuccessful due to the presence of large quantities of inorganic salts in the samples, which negatively impacted the ionization efficiencies of the products. Nevertheless, low-volatility products from both the •OH addition and the H-abstraction channels likely contributed to aqSOA formation for the four GLVs. Sarang et al. (2023) previously detected products formed from both channels in their study of the aqueous •OH oxidation of various GLVs. In the case of cHxO, the dominant products from the H-abstraction channel were reported to be at least 15 kcal mol^{-1} more stable than the products from the •OH-addition channel (Sarang et al., 2023). Subsequent density functional theory calculations indicated that both channels were important contributors to product formation due to the barrierless pathway in the •OH-addition channel and the formation of thermodynamically stable allylic alkyl radicals in the H-abstraction channel (Sarang et al., 2023). Allylic alkyl radicals from the H-abstraction channel similarly play important roles in product formation in the •OH oxidation of large unsaturated organic compounds (Nah et al., 2014).

In contrast to cHxO, tHxO, and tPtO, the Y_{SOA} values for MBO were not statistically different ($p > 0.05$) from 0 %. The substantial differences in the Y_{SOA} values for MBO vs. cHxO, tHxO, and tPtO could be attributed to the molecular structure of MBO. MBO contains a terminal C=C bond that is adjacent to its OH group, whereas cHxO, tHxO, and tPtO contain non-terminal C=C bonds that are non-adjacent to their OH groups (Fig. 1). Due to the molecular structure of MBO, the formation of RO• with oxygen radical centers adjacent to at least one OH functional group is enhanced for both the •OH-addition and H-abstraction channels (Fig. S9). Their close proximity to oxygenated functional groups increases the susceptibility of these RO• to fragmentation (Atkinson, 1997), which forms lower-molecular-weight compounds that may volatilize into the gas phase. Thus, the enhanced formation of RO• that preferentially fragments into higher-volatility products during the reaction of MBO with •OH under cloud-/fog-like conditions would explain its low Y_{SOA} values. In contrast, RO• formation (and, thus, fragmentation) is not enhanced in the •OH reactions of cHxO, tHxO, and tPtO due to the formation of primary

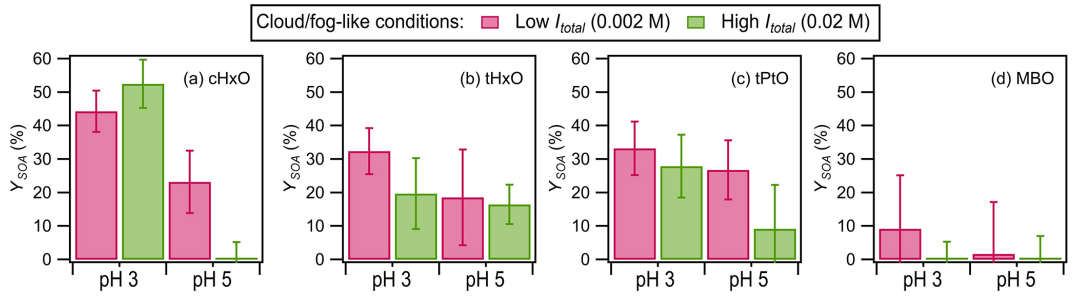

Figure 3. Y_{SOA} values for the four GLVs at one GLV lifetime during nitrate-mediated photooxidation under cloud-/fog-like conditions. The error bars represent 1 standard deviation originating from triplicate experiments and measurements and include errors propagated from the standard deviations of the sulfate concentrations measured by ACSM. The ACSM-measured organic signals for cHxO at pH 5 and $I_{total} = 0.02$ M and for MBO at pH 3 and 5 at $I_{total} = 0.02$ M and at pH 5 at $I_{total} = 0.002$ M were very low, resulting in close to zero organic concentrations and Y_{SOA} values. Therefore, there was essentially no formation of low-volatility products from these three experiments, and the Y_{SOA} values were essentially zero. Statistical analyses (Student's t test) on the differences in the Y_{SOA} values are presented in Tables S10 to S13.

and secondary RO_2• formed from the •OH-addition and H-abstraction channels.

Under the same ionic-strength conditions, the Y_{SOA} values for the four GLVs were generally higher at pH 3 than at pH 5, though these pH-dependent trends were not statistically significant ($p > 0.05$) in some instances (Tables S10 to S13). It is possible that the enhanced aqSOA formation at lower pH was due to acid-catalyzed reactions. The aqueous reaction of •OH with the four GLVs likely forms various higher- and lower-molecular-weight carbonyls (Figs. S8 and S9) (Sarang et al., 2021a, 2023). Some of these carbonyls could have undergone acid-catalyzed reactions (e.g., hydration, polymerization, aldol condensation) to form low-volatility products (Ervens et al., 2011; Maben and Ziemann, 2023; Presberg et al., 2024; Cooke et al., 2024). Additionally, it is possible that NO• enhanced the formation of low-volatility products that contributed to aqSOA at lower pH, possibly through the formation of low-volatility organonitrates via the $RO_2• + NO• \rightarrow RONO_2$ pathway (Atkinson and Arey, 2003). This is because NO• formation from nitrate photolysis would be enhanced at pH 3 (Table S1). HNO_2 is favored over its conjugated base NO_2^- at pH < 3.3 (Marussi and Vione, 2021). The production of NO• from the photolysis of HNO_2 (R15 in Table S1) is nearly 1 order of magnitude faster than its formation from NO_2^- photolysis (R10 in Table S1).

Interestingly, with the exception of cHxO at pH 3, the Y_{SOA} values for the four GLVs were higher at $I_{total} = 0.002$ M than at $I_{total} = 0.02$ M under the same pH conditions, though these ionic-strength-dependent trends were not statistically significant ($p > 0.05$) in some instances (Tables S10 to S13). This is in contrast to the insignificant effect that ionic strength had on k_{obs} (Fig. 2). $(NH_4)_2SO_4$ was used to control the ionic strengths of the solutions (Table 1). Thus, our results indicated that even though ionic strength and/or sulfate concentration had insignificant effects on the reaction kinetics under cloud-/fog-like conditions, they could significantly affect the formation of low-volatility products. The lower Y_{SOA} values measured at higher I_{total} and sulfate concentrations under the same pH conditions implied that fragmentation reactions that form volatile lower-molecular-weight products were enhanced at higher I_{total} and/or sulfate concentrations. Additionally, the higher-I_{total} conditions could have enhanced the partitioning of products into the gas phase due to the salting-out effect (Peng and Wan, 1998).

3.2 Aqueous-aerosol-like conditions

3.2.1 Reaction kinetics

Figure 4 shows the k_{obs} values for the four GLVs upon irradiation in the presence of nitrate at different pH levels (i.e., 3 vs. 5) and ionic strengths (i.e., 0.5 M vs. 3.3 M). The concentrations of the GLVs and NH_4NO_3 used in this set of experiments to simulate aqueous-aerosol-like conditions were both 100 times higher than those used to simulate cloud-/fog-like conditions while maintaining the same nitrate / GLV molar concentration ratio of 2.5 : 1 (Table 1). Separate experiments performed in the absence of GLVs and using BA as the •OH probe compound showed that the estimated $[•OH]_{ss}$ values decreased with pH under these cloud-/fog-like conditions (Fig. S7b), consistent with results for the cloud-/fog-like conditions (Fig. S7a). Unsurprisingly, the $[•OH]_{ss}$ values for aqueous-aerosol-like conditions were higher than those for the cloud-/fog-like conditions due to the higher concentrations of NH_4NO_3 used to simulate aqueous-aerosol-like conditions. The k_{obs} values for the four GLVs were on the orders of 10^{-6} to 10^{-3} s^{-1}.

The k_{obs} values measured for cHxO, tHxO, and tPtO under aqueous-aerosol-like conditions were factors of 1.1 to 6.1 lower than those measured for cloud-/fog-like conditions (Fig. 2). The lower k_{obs} values measured for these three GLVs under aqueous-aerosol-like conditions could be due, in

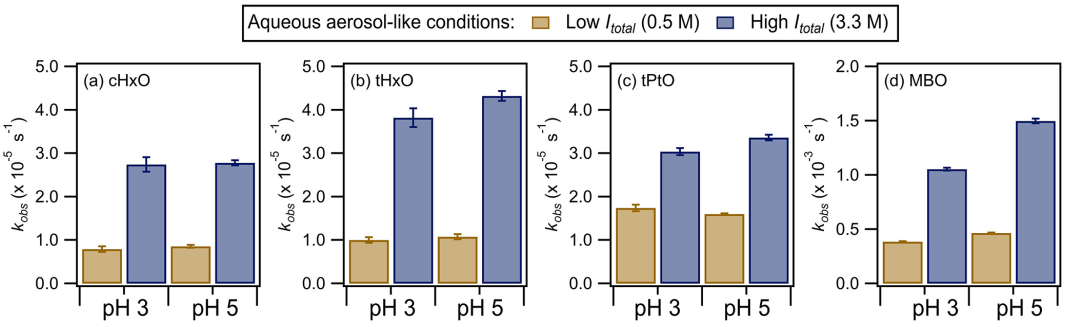

Figure 4. The k_{obs} values for the four GLVs during nitrate-mediated photooxidation under aqueous-aerosol-like conditions (Table 1). The error bars represent 1 standard deviation originating from triplicate experiments and measurements. Statistical analyses (Student's t test) on the differences in the k_{obs} values are presented in Tables S14 to S17.

part, to the exponential decrease in the nitrate photolysis rate with increasing nitrate concentration (Ye et al., 2017). Consequently, the production of reactive species does not increase linearly with the nitrate concentration. Additionally, sulfur-containing radicals and reactive species produced from sulfate photolysis are expected to contribute significantly to the degradation of the GLVs under aqueous-aerosol-like conditions due to the high concentration of $(NH_4)_2SO_4$ in the solutions (Cope et al., 2022). Work by Sarang et al. (2021b) suggests that the rate constants for the reactions of GLVs with $SO_4^{\bullet-}$ are about 1 order of magnitude lower than those of their reactions with •OH (Table S5). Nonetheless, the exponential decrease in the nitrate photolysis rate with increasing nitrate concentration does not completely explain the other noticeable differences in the k_{obs} results for aqueous-aerosol-like vs. cloud-/fog-like conditions. Firstly, the k_{obs} values for MBO under aqueous-aerosol-like conditions were factors of 1.2 to 5.1 higher than those under cloud-/fog-like conditions. Reasons for MBO's higher k_{obs} values under aqueous-aerosol-like conditions are currently unknown. Secondly, in contrast to the insignificant effect that the ionic strength and/or sulfate concentration had on the reaction kinetics under the same pH conditions for cloud-/fog-like conditions, the k_{obs} values for the four GLVs were significantly higher at $I_{total} = 3.3$ M than at $I_{total} = 0.5$ M ($p < 0.05$) under the same pH conditions for aqueous-aerosol-like conditions.

The higher k_{obs} values at higher I_{total} under the same pH conditions for aqueous-aerosol-like conditions could be due to higher •OH reactivities at higher ionic strength (Herrmann, 2003; Mekic and Gligorovski, 2021; Weller et al., 2010). Additionally, since $(NH_4)_2SO_4$ was used to control the ionic strengths of the solutions, sulfate photolysis likely contributed to the ionic-strength-dependent/sulfate-dependent k_{obs} trends for the aqueous-aerosol-like conditions (Table S4). Cope et al. (2022) showed that sulfur-containing radicals (e.g., $SO_4^{\bullet-}$) were formed in $(NH_4)_2SO_4$-containing concentrated solutions and aqueous aerosols when they were irradiated with UVB light or simulated sunlight. Even though the mechanism for the formation of sulfur-containing radicals from aqueous $(NH_4)_2SO_4$ photolysis remains unknown, the authors showed that the $SO_4^{\bullet-}$ formed could easily react with various organic compounds in aqueous aerosols. The $(NH_4)_2SO_4$ concentrations used in this study (0.16 and 1.09 M) were substantially lower than the $(NH_4)_2SO_4$ concentration used by Cope et al. (2022) (3.7 M). Nevertheless, sulfate photolysis occurred under this study's aqueous-aerosol-like conditions since the concentrations of the four GLVs decreased upon irradiation when only sulfate was present in the solutions (Fig. S10), likely driven primarily by their reactions with $SO_4^{\bullet-}$.

Our results clearly show that sulfur-containing radicals produced from sulfate photolysis can participate in aqueous reactions with GLVs in aqueous aerosols but not in cloud and fog droplets. This could be due to the low hydration numbers in aqueous aerosols that would reduce the energy needed to produce sulfur-containing radicals from sulfate photolysis (Cope et al., 2022; Xu et al., 1998). As explained by Cope et al. (2022), a fully solvated SO_4^{2-} anion in dilute solutions has about 16 water molecules in its first solvation shell (Plumridge et al., 2000). The energy needed to detach an electron from $SO_4^{2-}(H_2O)_n$ to produce $SO_4^{\bullet-}(H_2O)_n$ decreases with the number of water molecules in its hydration shell, and electron detachment potentially occurs spontaneously at 3 water molecules (Pathak, 2014). Thus, the effective potential barrier for the electron detachment of $SO_4^{2-}(H_2O)_4$ under concentrated conditions akin to aqueous aerosols is likely substantially lower compared to that under dilute conditions akin to those of cloud and fog droplets (Yang et al., 2002). Consequently, the likelihood of sulfur-containing radical production in concentrated aqueous aerosols would be substantially higher than that in diluted cloud and fog droplets.

Comparisons of the k_{obs} values obtained in the presence of sulfate and nitrate (Fig. 4) vs. only sulfate (Fig. S10) indicated that sulfate photolysis had a complex non-additive effect on the GLVs' reaction kinetics. Only approximately half of the k_{obs} values measured in the presence of sulfate and nitrate were significantly higher ($p < 0.05$) than those measured in the presence of only sulfate under the same pH con-

ditions. The non-additive effect that sulfate photolysis had on the GLVs' reaction kinetics could be due to its mechanism coupling with the nitrate photolysis mechanism. For instance, $SO_4{\bullet}^-$ could react with the NO_3^- anion to form $NO_3{\bullet}$ and the SO_4^{2-} anion (de Semainville et al., 2007). However, since the mechanism for the formation of sulfur-containing radicals from sulfate photolysis remains unknown, we were unable to assess the extent to which the sulfate photolysis mechanism coupled with the nitrate photolysis mechanism under our experimental conditions. Furthermore, contributions of the ·OH, $SO_4{\bullet}^-$, and $NO_3{\bullet}$ reactions to the measured k_{obs} would require knowledge of both the reaction rate constants and the concentrations of ·OH, $SO_4{\bullet}^-$, and $NO_3{\bullet}$. While the $SO_4{\bullet}^-$ and $NO_3{\bullet}$ concentrations in our study are not known, work by Richards-Henderson et al. (2014) and Sarang et al. (2021b) suggests that the rate constants for the reactions of GLVs with ·OH, $SO_4{\bullet}^-$, and $NO_3{\bullet}$ are on the orders of $10^9\,M^{-1}\,s^{-1}$, 10^8 to $10^9\,M^{-1}\,s^{-1}$, and 10^7 to $10^8\,M^{-1}\,s^{-1}$, respectively (Table S5). However, the aforementioned reaction rate constants were measured using dilute solutions with low ionic strengths (Sarang et al., 2021b), and it is unclear whether they could be extrapolated to aqueous aerosols which have high ionic strengths (Herrmann et al., 2015).

With the exception of tPtO at $I_{total} = 0.5\,M$, the k_{obs} values were higher at pH 5 than at pH 3 under the same ionic-strength conditions, though these pH-dependent trends were not statistically significant ($p > 0.05$) in some instances (Tables S14 to S17). The increase in k_{obs} with pH could potentially be due to the formation of ·OH, $SO_4{\bullet}^-$, and $NO_3{\bullet}$ from the coupled sulfate and nitrate photolysis mechanisms being pH-dependent, though this would require future studies to elucidate the mechanisms. The k_{obs} values measured in the presence of only sulfate did not have an obvious pH dependence (Fig. S10), which could be due to the four GLVs being pH-insensitive organic compounds. Cope et al. (2022) previously reported that pH had substantial effects on the reactions of $SO_4{\bullet}^-$ with pH-sensitive organic compounds but not on the reactions of $SO_4{\bullet}^-$ with pH-insensitive organic compounds.

3.2.2 Mass yields of aqSOA

Figure 5 shows the Y_{SOA} values for the four GLVs measured at one GLV lifetime during irradiation in the presence of nitrate at different pH levels (i.e., 3 vs. 5) and ionic strengths (i.e., 0.5 M vs. 3.3 M). The Y_{SOA} values measured under aqueous-aerosol-like conditions were substantially higher than those measured under cloud-/fog-like conditions (Fig. 3). The enhanced aqSOA formation under aqueous-aerosol-like conditions could be attributed to the higher concentrations of GLVs, which were 100 times higher than those used under cloud-/fog-like conditions. Consequently, the reaction of higher concentrations of GLVs enhanced $RO_2{\bullet}$ and RO• combination reactions that led to oligomer formation.

Similarly to the Y_{SOA} measured under cloud-/fog-like conditions (Fig. 3), the Y_{SOA} values for the four GLVs generally decreased with increasing pH under the same ionic-strength conditions and with increasing ionic strength and sulfate concentration under the same pH conditions, though these trends were not statistically significant ($p > 0.05$) in some instances (Tables S18 to S21). The enhanced aqSOA formation at lower pH could be due to the formation of low-volatility products from acid-catalyzed reactions (e.g., hydration, polymerization, aldol condensation) (Ervens et al., 2011; Maben and Ziemann, 2023; Presberg et al., 2024; Cooke et al., 2024) and/or the enhanced formation of low-volatility organonitrates via the $RO_2{\bullet} + NO{\bullet} \rightarrow RONO_2$ pathway (Atkinson and Arey, 2003). Reduced aqSOA formation at higher ionic strength and sulfate concentration was likely due to the enhancement of fragmentation pathways in the reactions of GLVs with sulfur-containing radicals formed from sulfate photolysis. For instance, $SO_4{\bullet}^-$ addition to C=C bonds to form higher-molecular-weight organosulfates is a minor channel compared to fragmentation pathways that form lower-molecular-weight products induced from electron transfer and other reactions by $SO_4{\bullet}^-$ (Ren et al., 2021). The higher concentrations of $SO_4{\bullet}^-$ formed from the photolysis of high concentrations of sulfate ($\geq 1085\,M$) likely enhanced fragmentation pathways that led to the formation of lower-molecular-weight products. Additionally, the higher-I_{total} conditions could have enhanced the partitioning of products into the gas phase due to the salting-out effect (Peng and Wan, 1998).

Most noticeably, Y_{SOA} values as high as 59 % were measured for MBO at $I_{total} = 0.5\,M$ under aqueous-aerosol-like conditions, in contrast to the substantially lower Y_{SOA} values measured under cloud-/fog-like conditions ($\leq 9\,\%$). While this could be due to the enhancement of $RO_2{\bullet}$ and RO• combination reactions induced by the higher concentrations of MBO in aqueous-aerosol-like conditions, the formation of low-volatility organosulfates induced by reactions involving sulfate could have contributed to the higher Y_{SOA} values as well. The concentrations of sulfate used to control the ionic strength in aqueous-aerosol-like conditions were up to 1861 times higher than those used in cloud-/fog-like conditions (Table 1). Thus, the reaction of MBO with sulfur-containing radicals formed from sulfate photolysis likely played a significant role in aqSOA formation under aqueous-aerosol-like conditions. Organosulfates (e.g., 2-hydroxy-2-methyl-4-sulfate-3-butanone) were previously identified as products from the reaction of MBO with $SO_4{\bullet}^-$ in the aqueous phase (Ren et al., 2021). Additionally, organosulfates could have been formed by acid-catalyzed reactions between sulfate and a MBO-derived epoxide (e.g., (3,3-dimethyloxiran-2-yl)methanol) formed from the ·OH reaction of MBO (Zhang et al., 2012). Nevertheless, increasing the sulfate concentration 7-fold to achieve $I_{total} = 3.3\,M$ led

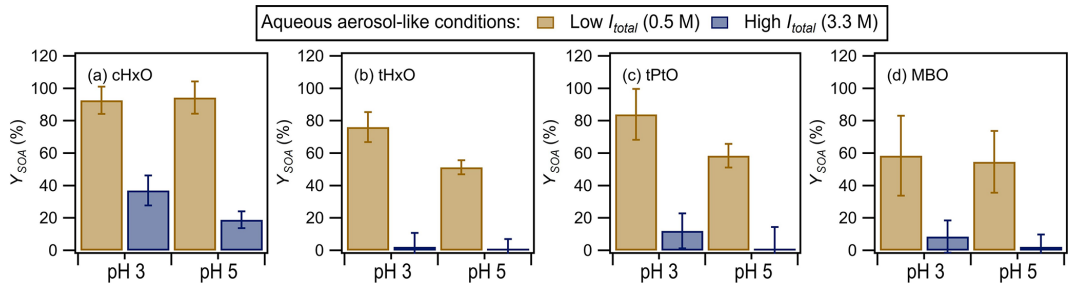

Figure 5. Y_{SOA} values for the four GLVs at one GLV lifetime during nitrate-mediated photooxidation under aqueous-aerosol-like conditions (Table 1). The error bars represent 1 standard deviation originating from triplicate experiments and measurements and include errors propagated from the standard deviations of the sulfate concentrations measured by ACSM. The ACSM-measured organic signals for tPtO at pH 5 at $I_{total} = 3.3$ M were very low, resulting in close to zero organic concentrations and Y_{SOA} values. Therefore, there was essentially no formation of low-volatility products from this experiment, and the Y_{SOA} value was essentially zero. Statistical analyses (Student's t test) on the differences in the Y_{SOA} values are presented in Tables S18 to S21.

to substantial reductions in Y_{SOA} (9 % and 2 %). This indicated that fragmentation pathways would eventually be enhanced in the reactions of GLVs with sulfur-containing radicals formed from the photolysis of high concentrations of sulfate.

4 Conclusions and implications

We investigated the nitrate-mediated photooxidation of four GLVs in dilute cloud-/fog-like and concentrated aqueous-aerosol-like conditions, focusing on the effects that pH, ionic strength, and sulfate on the reaction kinetics and aq-SOA mass yields. Our results showed that the aqueous reaction medium conditions governed the effects that pH, ionic strength, and sulfate had on the reaction kinetics and aq-SOA mass yields. Under dilute cloud-/fog-like conditions, the four GLVs had higher k_{obs} at lower pH, which could be attributed to the pH-dependent formation of •OH and other reactive species from nitrate photolysis. Ionic strength and sulfate had insignificant effects on k_{obs}. In contrast, under concentrated aqueous-aerosol-like conditions, the four GLVs had higher k_{obs} at higher pH, as well as higher k_{obs} values at higher ionic strength and sulfate concentration. Many of these differences could be attributed to sulfur-containing radicals produced from sulfate photolysis participating in the reactions of GLVs under aqueous-aerosol-like conditions but not in cloud-/fog-like conditions. Under cloud-/fog-like conditions where the sulfate concentrations were low, k_{obs} was governed by the reactions of GLVs with •OH and other reactive species from nitrate photolysis. In contrast, the high sulfate concentrations in the aqueous-aerosol-like conditions enhanced the formation of sulfur-containing radicals from sulfate photolysis, which participated in the reactions of GLVs. Higher Y_{SOA} values were measured under aqueous-aerosol-like conditions, likely due to enhanced oligomer formation from RO_2• and RO• combination reactions caused by the higher concentrations of GLVs reacted. Despite the different effects that pH, ionic strength, and sulfate had on the reaction kinetics in cloud-/fog-like vs. aqueous-aerosol-like conditions, similar Y_{SOA} trends were observed for these two reaction conditions. Higher Y_{SOA} was measured at lower pH, which could be due to the enhanced formation of low-volatility products from acid-catalyzed reactions and/or $RO_2\bullet + NO\bullet \rightarrow RONO_2$ reactions. Lower Y_{SOA} was measured at higher ionic strength and sulfate concentration, which could be attributed to the enhancement of fragmentation pathways in the reactions of GLVs with sulfur-containing radicals formed from sulfate photolysis.

Overall, the results provide new insights into the aqueous photooxidation of GLVs in areas with substantial levels of nitrate in cloud and fog droplets and aqueous aerosols. These insights are expected to be useful in modeling studies of the atmospheric fates of GLVs and their contributions to the SOA budget. These insights build upon those provided by previous studies that were conducted under dilute cloud-/fog-like conditions and in the absence of inorganic salts (Richards-Henderson et al., 2014, 2015; Sarang et al., 2021b, 2023). Results from this study highlight the influences that nitrate and sulfate, the two main inorganic constituents in cloud and fog droplets and aqueous aerosols in most regions, can have on the aqueous photooxidation of GLVs. Additionally, the magnitudes of their influences depend on the aqueous reaction medium (i.e., dilute cloud and fog droplets vs. concentrated aqueous aerosols) in which the reactions occur.

Our study also highlights many questions about the sulfate photolysis mechanism that need to be addressed in future studies. These include the mechanism for the formation of sulfur-containing radicals from aqueous $(NH_4)_2SO_4$ photolysis and how the sulfate photolysis mechanism can couple with the nitrate photolysis mechanism to affect the formation of reactive species including •OH. With the exception of pH 5 under aqueous-aerosol-like conditions, Fig. S7 shows that the $[\bullet OH]_{ss}$ generally decreased with increasing sulfate concentration, though the magnitude of the decrease

depended on the pH. Additional studies are needed to elucidate how the presence of sulfate will affect the formation of reactive species under different conditions (e.g., pH, ionic strength, aqueous reaction medium). While not investigated in this study due to our inability to completely remove inorganic salts prior to UPLC-MS analysis, we hypothesize that $[\bullet OH]_{ss}$ will likely similarly decrease with increasing sulfate concentration under concentrated aqueous-aerosol-like conditions. Additionally, even though this study focuses on the aqueous photooxidation of GLVs, it is likely that nitrate, sulfate, and the aqueous reaction medium will influence the aqueous photooxidation of other water-soluble organic compounds as well. More importantly, the manner in which nitrate and sulfate influence the reaction kinetics and aqSOA formation will depend on not only the aqueous reaction medium in which the reactions occur, but also whether the water-soluble organic compound is pH-sensitive or pH-insensitive (Cope et al., 2022; Lyu et al., 2023; Yang et al., 2023). The aforementioned factors need to be considered in future studies on the photooxidation of water-soluble organic compounds in different atmospheric aqueous phases.

There are several caveats that should be noted. First, we were unable to completely distinguish between the effects of sulfate and ionic strength on the aqueous photooxidation of GLVs since H_2SO_4 and $(NH_4)_2SO_4$ were used to control both the pH and ionic strength of the solutions. Second, the effects of only two ionic-strength conditions, 0.5 and 3.3 M, were investigated in experiments simulating aqueous aerosols. However, ionic strengths in atmospheric aqueous aerosols span a large range and can reach 45 M (Herrmann et al., 2015; Volkamer et al., 2007). Future studies could consider using a chemically inert inorganic salt (e.g., sodium perchlorate (Mekic et al., 2018a)) to control the ionic strength of solutions and investigate reactions in aqueous aerosols with very high ionic strengths. Third, many of our conclusions regarding key reaction pathways were drawn based on Y_{SOA} measurements performed using an ACSM due to our inability to completely remove inorganic salts from experimental samples before UPLC-MS analysis. Future studies should consider using alternative analytical methods that are not adversely impacted by inorganic salts (e.g., gas chromatography–mass spectrometry (Sarang et al., 2023) and nuclear magnetic resonance (Ren et al., 2021)) to identify prominent products and reaction pathways, though the detection of oligomers is still expected to be analytically challenging.

Data availability. The data used in this publication are available to the community and can be accessed either on request to the corresponding author or online at https://doi.org/10.5281/zenodo.14829906 (Nah, 2025).

Supplement. The supplement related to this article is available online at https://doi.org/10.5194/acp-25-10731-2025-supplement.

Author contributions. YL: conceptualization, investigation, and writing – original draft & editing. TJ: investigation, writing – review & editing. RM, MKEC, TZ, SY, CKW, and YG: investigation. YQ: writing – review & editing. TN: conceptualization, writing – review & editing, supervision. All authors reviewed the manuscript and agreed to the final version.

Competing interests. At least one of the (co-)authors is a member of the editorial board of *Atmospheric Chemistry and Physics*. The peer-review process was guided by an independent editor, and the authors also have no other competing interests to declare.

Disclaimer. Publisher's note: Copernicus Publications remains neutral with regard to jurisdictional claims made in the text, published maps, institutional affiliations, or any other geographical representation in this paper. While Copernicus Publications makes every effort to include appropriate place names, the final responsibility lies with the authors.

Acknowledgements. The authors thank Yuefei Phoebe Ruan and Jiajun Wu from the State Key Laboratory of Marine Environmental Health, City University of Hong Kong, for their technical support with the UPLC-MS measurements and analyses. Open access was made possible with partial support from the Open Access Publishing Fund of the City University of Hong Kong.

Financial support. The work described in this paper was supported by a grant from the Research Grants Council of the Hong Kong Special Administrative Region, China (project numbers 11303720 and 11303321).

Review statement. This paper was edited by Ryan Sullivan and reviewed by two anonymous referees.

References

Achtert, P., O'Connor, E. J., Brooks, I. M., Sotiropoulou, G., Shupe, M. D., Pospichal, B., Brooks, B. J., and Tjernström, M.: Properties of Arctic liquid and mixed-phase clouds from shipborne Cloudnet observations during ACSE 2014, Atmos. Chem. Phys., 20, 14983–15002, https://doi.org/10.5194/acp-20-14983-2020, 2020.

Ameye, M., Allmann, S., Verwaeren, J., Smagghe, G., Haesaert, G., Schuurink, R. C., and Audenaert, K.: Green leaf volatile production by plants: a meta-analysis, New Phytol., 220, 666–683, https://doi.org/10.1111/nph.14671, 2018.

Anastasio, C. and McGregor, K. G.: Chemistry of fog waters in California's Central Valley: 1. In situ photoformation of hy-

droxyl radical and singlet molecular oxygen, Atmos. Environ., 35, 1079–1089, https://doi.org/10.1016/S1352-2310(00)00281-8, 2001.

Arakaki, T., Miyake, T., Hirakawa, T., and Sakugawa, H.: pH Dependent Photoformation of Hydroxyl Radical and Absorbance of Aqueous-Phase N(III) (HNO_2 and NO_2^-), Environ. Sci. Technol., 33, 2561–2565, https://doi.org/10.1021/es980762i, 1999.

Atkinson, R.: Atmospheric reactions of alkoxy and β-hydroxyalkoxy radicals, Int. J. Chem. Kinet., 29, 99–111, https://doi.org/10.1002/(SICI)1097-4601(1997)29:2<99::AID-KIN3>3.0.CO;2-F, 1997.

Atkinson, R. and Arey, J.: Atmospheric degradation of volatile organic compounds, Chem. Rev., 103, 4605–4638, https://doi.org/10.1021/cr0206420, 2003.

Benson, S. W.: Thermochemical Kinetics: Methods for the Estimation of Thermochemical Data and Rate Parameters, in: 2nd Edn., Wiley, https://doi.org/10.1002/anie.197708831, 1976.

Bianco, A., Passananti, M., Brigante, M., and Mailhot, G.: Photochemistry of the Cloud Aqueous Phase: A Review, Molecules, 25, 423, https://doi.org/10.3390/molecules25020423, 2020.

Bielski, B. H. J., Cabelli, D. E., Arudi, R. L., and Ross, A. B.: Reactivity of HO_2 / O_2^- Radicals in Aqueous Solution, J. Phys. Chem. Ref. Data, 14, 1041–1100, https://doi.org/10.1063/1.555739, 1985.

Bzdek, B. R., Reid, J. P., and Cotterell, M. I.: Open questions on the physical properties of aerosols, Commun. Chem., 3, 105, https://doi.org/10.1038/s42004-020-00342-9, 2020.

Chen, G. D., Hanukovich, S., Chebeir, M., Christopher, P., and Liu, H. Z.: Nitrate Removal via a Formate Radical-Induced Photochemical Process, Environ. Sci. Technol., 53, 316–324, https://doi.org/10.1021/acs.est.8b04683, 2019.

Cofer, T. M., Engelberth, M., and Engelberth, J.: Green leaf volatiles protect maize (Zea mays) seedlings against damage from cold stress, Plant Cell Environ., 41, 1673–1682, https://doi.org/10.1111/pce.13204, 2018.

Cooke, M. E., Armstrong, N. C., Fankhauser, A. M., Chen, Y. Z., Lei, Z. Y., Zhang, Y., Ledsky, I. R., Turpin, B. J., Zhang, Z. F., Gold, A., McNeill, V. F., Surratt, J. D., and Ault, A. P.: Decreases in Epoxide-Driven Secondary Organic Aerosol Production under Highly Acidic Conditions: The Importance of Acid-Base Equilibria, Environ. Sci. Technol., 58, 10675–10684, https://doi.org/10.1021/acs.est.3c10851, 2024.

Cooper, W. J., Cramer, C. J., Martin, N. H., Mezyk, S. P., O'Shea, K. E., and von Sonntag, C.: Free Radical Mechanisms for the Treatment of Methyl-Butyl Ether (MTBE) via Advanced Oxidation/Reductive Processes in Aqueous Solutions, Chem. Rev., 109, 1302–1345, https://doi.org/10.1021/cr078024c, 2009.

Cope, J. D., Bates, K. H., Tran, L. N., Abellar, K. A., and Nguyen, T. B.: Sulfur radical formation from the tropospheric irradiation of aqueous sulfate aerosols, P. Natl. Acad. Sci. USA, 119, e2202857119, https://doi.org/10.1073/pnas.2202857119, 2022.

Daellenbach, K. R., Bozzetti, C., Krepelová, A. K., Canonaco, F., Wolf, R., Zotter, P., Fermo, P., Crippa, M., Slowik, J. G., Sosedova, Y., Zhang, Y., Huang, R. J., Poulain, L., Szidat, S., Baltensperger, U., El Haddad, I., and Prévôt, A. S. H.: Characterization and source apportionment of organic aerosol using offline aerosol mass spectrometry, Atmos. Meas. Tech., 9, 23–39, https://doi.org/10.5194/amt-9-23-2016, 2016.

de Semainville, P. G., Hoffmann, D., George, C., and Herrmann, H.: Study of nitrate radical (NO_3) reactions with carbonyls and acids in aqueous solution as a function of temperature, Phys. Chem. Chem. Phys., 9, 958–968, https://doi.org/10.1039/b613956f, 2007.

Dickson, A. G., Wesolowski, D. J., Palmer, D. A., and Mesmer, R. E.: Dissociation-Constant of Bisulfate Ion in Aqueous Sodium-Chloride Solutions to 250-Degrees-C, J. Phys. Chem., 94, 7978–7985, https://doi.org/10.1021/j100383a042, 1990.

Ervens, B., Turpin, B. J., and Weber, R. J.: Secondary organic aerosol formation in cloud droplets and aqueous particles (aqSOA): a review of laboratory, field and model studies, Atmos. Chem. Phys., 11, 11069–11102, https://doi.org/10.5194/acp-11-11069-2011, 2011.

Ford, E., Hughes, M. N., and Wardman, P.: Kinetics of the reactions of nitrogen dioxide with glutathione, cysteine, and uric acid at physiological pH, Free Radical Biol. Med., 32, 1314–1323, https://doi.org/10.1016/S0891-5849(02)00850-X, 2002.

García-Plazaola, J. I., Portillo-Estrada, M., Fernández-Marín, B., Kännaste, A., and Niinemets, Ü.: Emissions of carotenoid cleavage products upon heat shock and mechanical wounding from a foliose lichen, Environ. Exp. Bot., 133, 87–97, https://doi.org/10.1016/j.envexpbot.2016.10.004, 2017.

Gen, M. S., Liang, Z. C., Zhang, R. F., Mabato, B. R. G., and Chan, C. K.: Particulate nitrate photolysis in the atmosphere, Environ. Sci.-Atmos., 2, 111–127, https://doi.org/10.1039/d1ea00087j, 2022.

Guenther, A. B., Jiang, X., Heald, C. L., Sakulyanontvittaya, T., Duhl, T., Emmons, L. K., and Wang, X.: The Model of Emissions of Gases and Aerosols from Nature version 2.1 (MEGAN2.1): an extended and updated framework for modeling biogenic emissions, Geosci. Model Dev., 5, 1471–1492, https://doi.org/10.5194/gmd-5-1471-2012, 2012.

Hamilton, J. F., Lewis, A. C., Carey, T. J., Wenger, J. C., Borrás i Garcia, E., and Muñoz, A.: Reactive oxidation products promote secondary organic aerosol formation from green leaf volatiles, Atmos. Chem. Phys., 9, 3815–3823, https://doi.org/10.5194/acp-9-3815-2009, 2009.

Harvey, R. M., Zahardis, J., and Petrucci, G. A.: Establishing the contribution of lawn mowing to atmospheric aerosol levels in American suburbs, Atmos. Chem. Phys., 14, 797–812, https://doi.org/10.5194/acp-14-797-2014, 2014.

Heald, C. L., Collett Jr, J. L., Lee, T., Benedict, K. B., Schwandner, F. M., Li, Y., Clarisse, L., Hurtmans, D. R., Van Damme, M., Clerbaux, C., Coheur, P. F., Philip, S., Martin, R. V., and Pye, H. O. T.: Atmospheric ammonia and particulate inorganic nitrogen over the United States, Atmos. Chem. Phys., 12, 10295–10312, https://doi.org/10.5194/acp-12-10295-2012, 2012.

Herrmann, H.: Kinetics of aqueous phase reactions relevant for atmospheric chemistry, Chem. Rev., 103, 4691–4716, https://doi.org/10.1021/cr020658q, 2003.

Herrmann, H., Hoffmann, D., Schaefer, T., Bräuer, P., and Tilgner, A.: Tropospheric Aqueous-Phase Free-Radical Chemistry: Radical Sources, Spectra, Reaction Kinetics and Prediction Tools, Chem. Phys. Chem., 11, 3796–3822, https://doi.org/10.1002/cphc.201000533, 2010.

Herrmann, H., Schaefer, T., Tilgner, A., Styler, S. A., Weller, C., Teich, M., and Otto, T.: Tropospheric Aqueous-Phase Chemistry: Kinetics, Mechanisms, and Its Coupling to

a Changing Gas Phase, Chem. Rev., 115, 4259–4334, https://doi.org/10.1021/cr500447k, 2015.

Jaoui, M., Kleindienst, T. E., Offenberg, J. H., Lewandowski, M., and Lonneman, W. A.: SOA formation from the atmospheric oxidation of 2-methyl-3-buten-2-ol and its implications for $PM_{2.5}$, Atmos. Chem. Phys., 12, 2173–2188, https://doi.org/10.5194/acp-12-2173-2012, 2012.

Jardine, K. J., Chambers, J. Q., Holm, J., Jardine, A. B., Fontes, C. G., Zorzanelli, R. F., Meyers, K. T., De Souza, V. F., Garcia, S., Gimenez, B. O., Piva, L. R. d. O., Higuchi, N., Artaxo, P., Martin, S., and Manzi, A. O.: Green Leaf Volatile Emissions during High Temperature and Drought Stress in a Central Amazon Rainforest, Plants, 4, 678–690, 2015.

Jiang, W. Q., Niedek, C., Anastasio, C., and Zhang, Q.: Photoaging of phenolic secondary organic aerosol in the aqueous phase:evolution of chemical and optical properties and effects of oxidants, Atmos. Chem. Phys., 23, 7103–7120, https://doi.org/10.5194/acp-23-7103-2023, 2023.

Joo, T., Chen, Y., Xu, W., Croteau, P., Canagaratna, M. R., Gao, D., Guo, H., Saavedra, G., Kim, S. S., Sun, Y., Weber, R., Jayne, J., and Ng, N. L.: Evaluation of a New Aerosol Chemical Speciation Monitor (ACSM) System at an Urban Site in Atlanta, GA: The Use of Capture Vaporizer and $PM_{2.5}$ Inlet, ACS Earth Space Chem., 5, 2565–2576, https://doi.org/10.1021/acsearthspacechem.1c00173, 2021.

Kim, S., Rickard, C., Hernandez-Vazquez, J., and Fernandez, D.: Early Night Fog Prediction Using Liquid Water Content Measurement in the Monterey Bay Area, Atmosphere, 13, 1332, https://doi.org/10.3390/atmos13081332, 2022.

Korolev, A. V., Isaac, G. A., Strapp, J. W., Cober, S. G., and Barker, H. W.: measurements of liquid water content profiles in midlatitude stratiform clouds, Q. J. Roy. Meteorol. Soc., 133, 1693–1699, https://doi.org/10.1002/qj.147, 2007.

Li, T., Wang, Z., Wang, Y. R., Wu, C., Liang, Y. H., Xia, M., Yu, C., Yun, H., Wang, W. H., Wang, Y., Guo, J., Herrmann, H., and Wang, T.: Chemical characteristics of cloud water and the impacts on aerosol properties at a subtropical mountain site in Hong Kong SAR, Atmos. Chem. Phys., 20, 391–407, https://doi.org/10.5194/acp-20-391-2020, 2020.

Lyu, Y., Chow, J. T. C., and Nah, T.: Kinetics of the nitrate-mediated photooxidation of monocarboxylic acids in the aqueous phase, Environ. Sci.-Proc. Imp., 25, 461–471, https://doi.org/10.1039/d2em00458e, 2023.

Ma, L., Guzman, C., Niedek, C., Tran, T., Zhang, Q., and Anastasio, C.: Kinetics and Mass Yields of Aqueous Secondary Organic Aerosol from Highly Substituted Phenols Reacting with a Triplet Excited State, Environ. Sci. Technol., 55, 5772–5781, https://doi.org/10.1021/acs.est.1c00575, 2021.

Maben, H. K. and Ziemann, P. J.: Kinetics of oligomer-forming reactions involving the major functional groups present in atmospheric secondary organic aerosol particles, Environ. Sci.-Proc. Imp., 25, 214–228, https://doi.org/10.1039/d2em00124a, 2023.

Mack, J. and Bolton, J. R.: Photochemistry of nitrite and nitrate in aqueous solution: a review, J. Photochem. Photobiol. A, 128, 1–13, https://doi.org/10.1016/S1010-6030(99)00155-0, 1999.

Marussi, G. and Vione, D.: Secondary Formation of Aromatic Nitroderivatives of Environmental Concern: Photonitration Processes Triggered by the Photolysis of Nitrate and Nitrite Ions in Aqueous Solution, Molecules, 26, 2550, https://doi.org/10.3390/molecules26092550, 2021.

Matsui, K. and Engelberth, J.: Green Leaf Volatiles – The Forefront of Plant Responses Against Biotic Attack, Plant Cell Physiol., 63, 1378–1390, https://doi.org/10.1093/pcp/pcac117, 2022.

Mekic, M. and Gligorovski, S.: Ionic strength effects on heterogeneous and multiphase chemistry: Clouds versus aerosol particles, Atmos. Environ., 244, 117911, https://doi.org/10.1016/j.atmosenv.2020.117911, 2021.

Mekic, M., Brigante, M., Vione, D., and Gligorovski, S.: Exploring the ionic strength effects on the photochemical degradation of pyruvic acid in atmospheric deliquescent aerosol particles, Atmos. Environ., 185, 237–242, https://doi.org/10.1016/j.atmosenv.2018.05.016, 2018a.

Mekic, M., Loisel, G., Zhou, W., Jiang, B., Vione, D., and Gligorovski, S.: Ionic-Strength Effects on the Reactive Uptake of Ozone on Aqueous Pyruvic Acid: Implications for Air–Sea Ozone Deposition, Environ. Sci. Technol., 52, 12306–12315, https://doi.org/10.1021/acs.est.8b03196, 2018b.

Mentel, T. F., Kleist, E., Andres, S., Dal Maso, M., Hohaus, T., Kiendler-Scharr, A., Rudich, Y., Springer, M., Tillmann, R., Uerlings, R., Wahner, A., and Wildt, J.: Secondary aerosol formation from stress-induced biogenic emissions and possible climate feedbacks, Atmos. Chem. Phys., 13, 8755–8770, https://doi.org/10.5194/acp-13-8755-2013, 2013.

Nah, T., Zhang, H., Worton, D. R., Ruehl, C. R., Kirk, B. B., Goldstein, A. H., Leone, S. R., and Wilson, K. R.: Isomeric Product Detection in the Heterogeneous Reaction of Hydroxyl Radicals with Aerosol Composed of Branched and Linear Unsaturated Organic Molecules, J. Phys. Chem. A, 118, 11555–11571, https://doi.org/10.1021/jp508378z, 2014.

Nah, T.: Dataset for paper "Roles of pH, ionic strength, and sulfate in the aqueous nitrate-mediated photooxidation of green leaf volatiles", Zenodo [data set] https://doi.org/10.5281/zenodo.14829906, 2025.

Nguyen, T. K. V., Zhang, Q., Jimenez, J. L., Pike, M., and Carlton, A. G.: Liquid Water: Ubiquitous Contributor to Aerosol Mass, Environ. Sci. Technol. Lett., 3, 257–263, https://doi.org/10.1021/acs.estlett.6b00167, 2016.

Pathak, A. K.: Conductance and bulk vertical detachment energy of hydrated sulphate and oxalate dianions: a theoretical study, Molecul. Phys., 112, 1548–1552, https://doi.org/10.1080/00268976.2013.843035, 2014.

Peng, J. and Wan, A.: Effect of ionic strength on Henry's constants of volatile organic compound, Chemosphere, 36, 2731–2740, https://doi.org/10.1016/S0045-6535(97)10232-6, 1998.

Plumridge, T. H., Steel, G., and Waigh, R. D.: Geometry-based simulation of the hydration of small molecules, Phys. Chem. Comm., 3, 36–41, https://doi.org/10.1039/B003723K, 2000.

Presberg, S. S., Waters, C. M., Lyon, S. A., and Elrod, M. J.: Thermodynamics and Kinetics of Atmospherically Relevant Acetalization Reactions, ACS Earth Space Chem., 8, 1634–1645, https://doi.org/10.1021/acsearthspacechem.4c00136, 2024.

Pye, H. O. T., Nenes, A., Alexander, B., Ault, A. P., Barth, M. C., Clegg, S. L., Collett, J. L., Fahey, K. M., Hennigan, C. J., Herrmann, H., Kanakidou, M., Kelly, J. T., Ku, I. T., McNeill, V. F., Riemer, N., Schaefer, T., Shi, G. L., Tilgner, A., Walker, J. T., Wang, T., Weber, R., Xing, J., Zaveri, R. A., and Zuend, A.: The acidity of atmospheric particles and clouds, At-

mos. Chem. Phys., 20, 4809–4888, https://doi.org/10.5194/acp-20-4809-2020, 2020.

Ren, H., Sedlak, J. A., and Elrod, M. J.: General Mechanism for Sulfate Radical Addition to Olefinic Volatile Organic Compounds in Secondary Organic Aerosol, Environ. Sci. Technol., 55, 1456–1465, https://doi.org/10.1021/acs.est.0c05256, 2021.

Richards-Henderson, N. K., Hansel, A. K., Valsaraj, K. T., and Anastasio, C.: Aqueous oxidation of green leaf volatiles by hydroxyl radical as a source of SOA: Kinetics and SOA yields, Atmos. Environ., 95, 105–112, https://doi.org/10.1016/j.atmosenv.2014.06.026, 2014.

Richards-Henderson, N. K., Pham, A. T., Kirk, B. B., and Anastasio, C.: Secondary Organic Aerosol from Aqueous Reactions of Green Leaf Volatiles with Organic Triplet Excited States and Singlet Molecular Oxygen, Environ. Sci. Technol., 49, 268–276, https://doi.org/10.1021/es503656m, 2015.

Sander, R.: Compilation of Henry's law constants (version 5.0.0) for water as solvent, Atmos, Chem, Phys,, 23, 10901–12440, https://doi.org/10.5194/acp-23-10901-2023, 2023.

Sarang, K., Rudzinski, K. J., and Szmigielski, R.: Green Leaf Volatiles in the Atmosphere-Properties, Transformation, and Significance, Atmosphere, 12, 1655, https://doi.org/10.3390/atmos12121655, 2021a.

Sarang, K., Otto, T., Rudzinski, K., Schaefer, T., Grgic, I., Nestorowicz, K., Herrmann, H., and Szmigielski, R.: Reaction Kinetics of Green Leaf Volatiles with Sulfate, Hydroxyl, and Nitrate Radicals in Tropospheric Aqueous Phase, Environ. Sci. Technol., 55, 13666–13676, https://doi.org/10.1021/acs.est.1c03276, 2021b.

Sarang, K., Otto, T., Gagan, S., Rudzinski, K., Schaefer, T., Brüggemann, M., Grgic, I., Kubas, A., Herrmann, H., and Szmigielski, R.: Aqueous-phase photo-oxidation of selected green leaf volatiles initiated by OH radicals: Products and atmospheric implications, Sci. Total Environ., 879, 162622, https://doi.org/10.1016/j.scitotenv.2023.162622, 2023.

Schaap, M., van Loon, M., ten Brink, H. M., Dentener, F. J., and Builtjes, P. J. H.: Secondary inorganic aerosol simulations for Europe with special attention to nitrate, Atmos. Chem. Phys., 4, 857–874, https://doi.org/10.5194/acp-4-857-2004, 2004.

Silva, D. B., Urbaneja, A., and Pérez-Hedo, M.: Response of mirid predators to synthetic herbivore-induced plant volatiles, Entomol. Exp. Appl., 169, 125–132, https://doi.org/10.1111/eea.12970, 2021.

Sindelarova, K., Granier, C., Bouarar, I., Guenther, A., Tilmes, S., Stavrakou, T., Müller, J. F., Kuhn, U., Stefani, P., and Knorr, W.: Global data set of biogenic VOC emissions calculated by the MEGAN model over the last 30 years, Atmos.Chem. Phys., 14, 9317–9341, https://doi.org/10.5194/acp-14-9317-2014, 2014.

Su, Q., Yang, F., Zhang, Q., Tong, H., Hu, Y., Zhang, X., Xie, W., Wang, S., Wu, Q., and Zhang, Y.: Defence priming in tomato by the green leaf volatile (*Z*)-3-hexenol reduces whitefly transmission of a plant virus, Plant Cell Environ., 43, 2797–2811, https://doi.org/10.1111/pce.13885, 2020.

Tilgner, A., Schaefer, T., Alexander, B., Barth, M., Collett, J. L., Fahey, K. M., Nenes, A., Pye, H. O. T., Herrmann, H., and McNeill, V. F.: Acidity and the multiphase chemistry of atmospheric aqueous particles and clouds, Atmos. Chem. Phys., 21, 13483–13536, https://doi.org/10.5194/acp-21-13483-2021, 2021.

US EPA: Estimation Programs Interface Suite™ for Microsoft® Windows, v 4.11 [code], https://www.epa.gov/tsca-screening-tools/epi-suitetm-estimation-program-interface#:~:text=TheEPI(EstimationProgramsInterface,(SRC) (last access: 15 September 2025), 2024.

Volkamer, R., San Martini, F., Molina, L. T., Salcedo, D., Jimenez, J. L., and Molina, M. J.: A missing sink for gas-phase glyoxal in Mexico City: Formation of secondary organic aerosol, Geophys. Res. Lett., 34, 19, https://doi.org/10.1029/2007GL030752, 2007.

Weller, C., Hoffmann, D., Schaefer, T., and Herrmann, H.: Temperature and Ionic Strength Dependence of NO-radical Reactions with Substituted Phenols in Aqueous Solution, Z. Phys. Chem., 224, 1261–1287, https://doi.org/10.1524/zpch.2010.6151, 2010.

West, J. J., Ansari, A. S., and Pandis, S. N.: Marginal PM_{25}: Nonlinear Aerosol Mass Response to Sulfate Reductions in the Eastern United States, J. Air Waste Manage. Assoc., 49, 1415–1424, https://doi.org/10.1080/10473289.1999.10463973, 1999.

Xu, J., Imre, D., McGraw, R., and Tang, I.: Ammonium Sulfate: Equilibrium and Metastability Phase Diagrams from 40 to −50 °C, J. Phys. Chem. B, 102, 7462–7469, https://doi.org/10.1021/jp981929x, 1998.

Xu, W., Lambe, A., Silva, P., Hu, W., Onasch, T., Williams, L., Croteau, P., Zhang, X., Renbaum-Wolff, L., Fortner, E., Jimenez, J. L., Jayne, J., Worsnop, D., and Canagaratna, M.: Laboratory evaluation of species-dependent relative ionization efficiencies in the Aerodyne Aerosol Mass Spectrometer, Aerosol Sci. Tech., 52, 626–641, https://doi.org/10.1080/02786826.2018.1439570, 2018.

Yang, J., Au, W. C., Law, H., Lam, C. H., and Nah, T.: Formation and evolution of brown carbon during aqueous-phase nitrate-mediated photooxidation of guaiacol and 5-nitroguaiacol, Atmos. Environ., 254, 118401, https://doi.org/10.1016/j.atmosenv.2021.118401, 2021.

Yang, J., Au, W. C., Law, H., Leung, C. H., Lam, C. H., and Nah, T.: pH affects the aqueous-phase nitrate-mediated photooxidation of phenolic compounds: implications for brown carbon formation and evolution, Environ. Sci.-Proc. Imp., 25, 176–189, https://doi.org/10.1039/d2em00004k, 2023.

Yang, X., Wang, X.-B., and Wang, L.-S.: Photodetachment of Hydrated Sulfate Doubly Charged Anions: $SO_4^{2-}(H_2O)_n$ $(n = 4–40)$†, J. Phys. Chem. A, 106, 7607–7616, https://doi.org/10.1021/jp014632z, 2002.

Ye, C. X., Zhang, N., Gao, H. L., and Zhou, X. L.: Photolysis of Particulate Nitrate as a Source of HONO and NO, Environ. Sci. Technol., 51, 6849–6856, https://doi.org/10.1021/acs.est.7b00387, 2017.

Zhang, H. F., Worton, D. R., Lewandowski, M., Ortega, J., Rubitschun, C. L., Park, J. H., Kristensen, K., Campuzano-Jost, P., Day, D. A., Jimenez, J. L., Jaoui, M., Offenberg, J. H., Kleindienst, T. E., Gilman, J., Kuster, W. C., de Gouw, J., Park, C., Schade, G. W., Frossard, A. A., Russell, L., Kaser, L., Jud, W., Hansel, A., Cappellin, L., Karl, T., Glasius, M., Guenther, A., Goldstein, A. H., Seinfeld, J. H., Gold, A., Kamens, R. M., and Surratt, J. D.: Organosulfates as Tracers for Secondary Organic Aerosol (SOA) Formation from 2-Methyl-3-Buten-2-ol (MBO) in the Atmosphere, Environ. Sci. Technol., 46, 9437–9446, https://doi.org/10.1021/es301648z, 2012.

Zhang, R. F., Gen, M. S., Fu, T. M., and Chan, C. K.: Production of Formate via Oxidation of Glyoxal Promoted by Particulate Nitrate Photolysis, Environ. Sci. Technol., 55, 5711–5720, https://doi.org/10.1021/acs.est.0c08199, 2021.

Zhou, W., Mekic, M., Liu, J., Loisel, G., Jin, B., Vione, D., and Gligorovski, S.: Ionic strength effects on the photochemical degradation of acetosyringone in atmospheric deliquescent aerosol particles, Atmos. Environ., 198, 83–88, https://doi.org/10.1016/j.atmosenv.2018.10.047, 2019.